Frequency-Domain Method for Flutter on a Highly Deformed Wing

Rodrigo Gaspar Pinto Ramos Correia

rodrigo.r.correia@tecnico.ulisboa.pt

Instituto Superior Técnico, Universidade de Lisboa, Portugal

November, 2020

Abstract

The objective of this work is to build a frequency domain tool through the assembly of already existing frameworks, which performs a flutter analysis on high aspect-ratio wings where the deformed wing configurations and its influence over the flutter speed are taken into account. From a Nonlinear Aeroelastic Framework, the tool gets as input the wing nonlinear aeroelastic static equilibrium positions and through a MATLAB code builds the structural and aerodynamic models (based on the Euler-Bernoulli Beam Theory and on the Doublet-Lattice Panel Method, respectively). Then, the solver NASTRAN performs the aeroelastic analyses by applying the p-k method at those equilibrium positions. These analyses are performed in an iterative cycle, so it is possible to take into account the wing deformation due to the airspeed while calculating the flutter speed. The obtained updated flutter speed is then compared with one calculated by a time domain approach. This comparison showed that despite some identical trends in both approaches, it was not possible to predict exactly the same flutter speed in both techniques. Still, it could be concluded that the developed frequency domain tool managed to produce consistent results at a low computational cost.

Keywords: Aeroelasticity; flutter; frequency-domain; geometric nonlinearities; high aspect-ratio wings.

1. Introduction

Over the years, with the goal of pursuing more efficient aircraft solutions, one of the most studied aircraft configurations has been high aspect-ratio wings. However, despite the aerodynamic benefit that grants a higher lift-to-drag ratio and a longer range to the aircraft, there are a few structural disadvantages related to this configuration, such as higher wing flexibility. This increase in wing flexibility while keeping a light structure leads to large deformations at normal operating conditions, which in turn results in the occurrence of aeroelastic effects on such wing, at a lower speed than in a stiffer wing [1]. Flutter is one of the most risky aeroelastic phenomena and it is generally the key focus of analysis in the aeroelasticity field.

In cases where structural nonlinearities are likely to occur, such as in highly flexible wings, the accuracy of time domain methods is usually higher than that of frequency domain methods [2],

which may reflect on the determination of the flutter speed. However, time domain methods carry several disadvantages, like a higher computational cost and a more complex interpretation of the results, which make the application of such type of methods to aircraft design and optimization problems quite impracticable. Unlike time domain methods, frequency domain methods can be run with a lower computational cost and be easier to apply to an optimization or an aircraft design problem. Although in highly flexible wings, because of the nonlinearities that may cause flutter at lower speeds than what linear analyses predict, the frequency domain methods need to be accordingly updated in order to accurately predict the flutter phenomenon.

There are not many studies in the literature [3] [4] which compare these two approaches for predicting flutter speeds and, in fact, the author did not find any which featured a comparison for highly flexible wing structures, where the geometrical nonlinearities would play an important role. Therefore, there would be value in developing an updated frequency domain tool where the deformed wing configurations and its influence over the flutter speed are taken into account, with the goal of accurately estimating the flutter speed of high aspect-ratio wings and comparing its results to those produced by a time domain method. This is the objective of this work.

2. Methodology

The aeroelastic phenomenon results from the interaction of aerodynamic, inertial and elastic forces [5]. A typical way of presenting such interaction is to describe the aeroelastic problem as a system of second-order differential equations in terms of its degrees of freedom $\{q\}$:

$$[M]\{\ddot{q}\} + [C]\{\dot{q}\} + [K]\{q\} = \{F\} \tag{1}$$

where $[M]$, $[C]$ and $[K]$ respectively represent the mass, damping and stiffness matrices of the system's structure; and $\{F\}$ represents the total load vector. The aeroelastic problem shown in the equation above can be considered as either steady or unsteady.

Both unsteady and steady analysis can be run in the Nonlinear Aeroelastic Framework developed by the IST Aerospace Group [6] [7] in order to generate the time domain results, as well as the wing converged positions of stationary equilibrium that serve as input for the frequency domain tool. In this framework, a Fluid-Structure Interaction (FSI) algorithm was implemented to couple the structural component of the model (a condensed 3D beam model) with the aerodynamic component of the model (a 3D panel code method) for nonlinear unsteady and steady analyses.

The nonlinear unsteady analyses, which estimate the wing's flutter speed based on the aeroelastic response to a prescribed gust at a given time interval, constitute the time domain approach. And for this work, these unsteady simulations are only used for comparison purposes with the updated frequency domain methodology.

On the other hand, the steady simulations are carried out to provide a position of stationary equilibrium, where the structural and the aerodynamic meshes converge, to the updated frequency domain method. These converged positions of stationary equilibrium are what feeds the frequency domain analysis tool, which will be summarized in the next chapter. This frequency domain tool resorts to a MATLAB code which generates the whole frequency domain analysis. It

takes as input the wing converged positions and from there it builds the structural and aerodynamic models. The structural model is an one-dimensional cantilever beam based on the Euler-Bernoulli Beam Theory [8], while the aerodynamic model is a 2D aerodynamic panel method grounded on the Doublet-Lattice Panel Method [9]. Then, on these models, the solver NASTRAN performs the aeroelastic analyses, calculating the flutter speed by applying the p-k method at the nonlinear aeroelastic static equilibrium position. These analyses are performed in an iterative cycle, so it is possible to take into account the wing deformation due to the airspeed while calculating the flutter speed. We so obtain the updated flutter speed, to be then compared with the one calculated by the time domain approach.

3. The Frequency Domain Analysis Tool

As introduced before, all the input wing configuration data we have for the frequency domain analysis comes from the Nonlinear Aeroelastic Framework. It carries out steady simulations to provide converged positions of the stationary equilibrium to the updated frequency domain method. These converged positions, for different wind speeds and angles of attack for the different aspect-ratio wings, will provide the several deformed wing configurations that will constitute the file database to be used as input in the frequency domain analysis tool.

The MATLAB code receives the deformed wing configurations generated by the FSI Solver and its inertial properties as inputs, and then builds the structural and aerodynamic components of the wing models on input files to be analyzed with NASTRAN.

This NASTRAN analysis calculates a flutter speed for each air speed and its correspondent deformed structure configuration. Finally, the program proceeds to find the actual flutter speed for the aspect-ratio and angle of attack combination in focus, by running this analysis in an iterative process to try to converge the wind and flutter speeds. This way, it is possible to use a frequency domain approach to find the flutter speed for a certain wing configuration, while taking into account its deformation due to the airspeed.

More specifically, the developed MATLAB tool is constituted by 5 functions (Figure 1). The main function, flutter.m, (Figure 2) runs the main iterative calculation routine, which in each cycle resorts to the flutter_SOL145.m function to find the flutter speed for a specific input airspeed and matching wing configuration. The main function also contains the flutter_param.m function, which has some analysis parameters, as well as the interpolate_deflections.m function (Figure 3), which in each cycle interpolates a new deformed wing configuration for the required input airspeed. Then, in each cycle run, the flutter_SOL145.m (Figure 4) function runs the NASTRAN flutter analysis for a specific input airspeed and corresponding deformed wing configuration. It writes the Nastran input file, runs NASTRAN, reads the result file, plots V-G and V-F graphs, analyzes the results and returns the estimated flutter speeds, as well as the corresponding frequencies and vibration modes. It also resorts to the beamwriter.m function (Figure 5) to build both the structural and the aerodynamic components of the beam model that will simulate the required wing configuration.

The diagram and flowcharts below aim to help understanding the structure of the frequency domain analysis tool. An overview of this updated frequency domain tool is depicted in Figure 1, while in Figures 2 to 5 each main function of this tool is detailed.

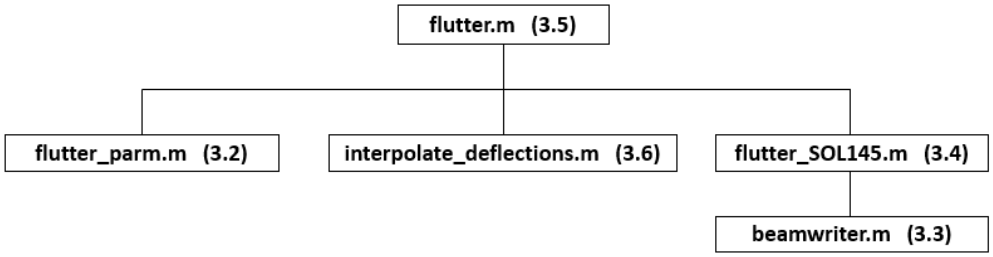

Figure 1 - Function structure of the Tool

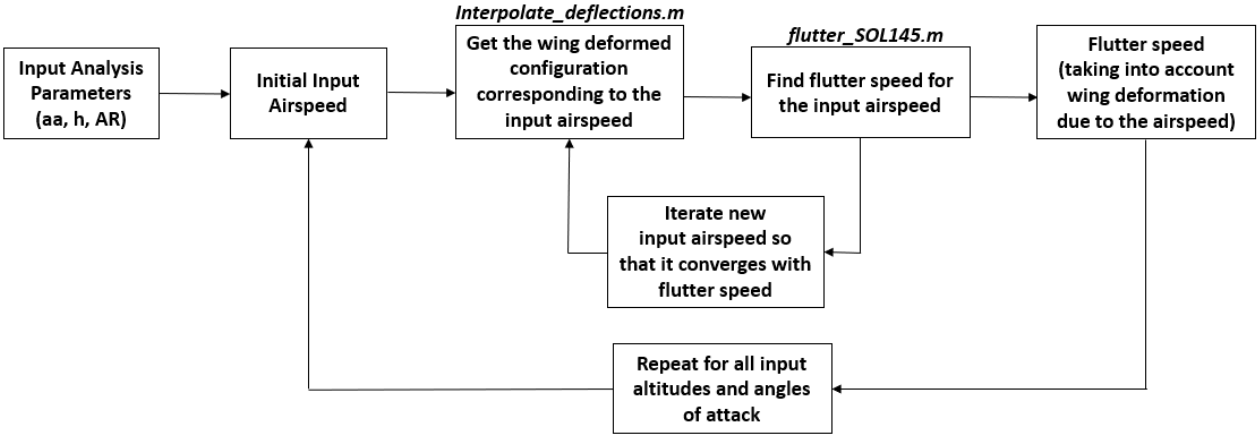

Figure 2 - flutter.m function flowchart

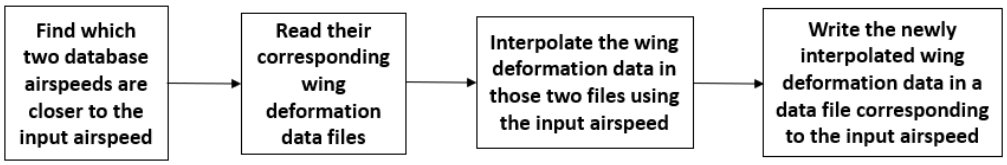

Figure 3 – interpolate_deflections.m function flowchart

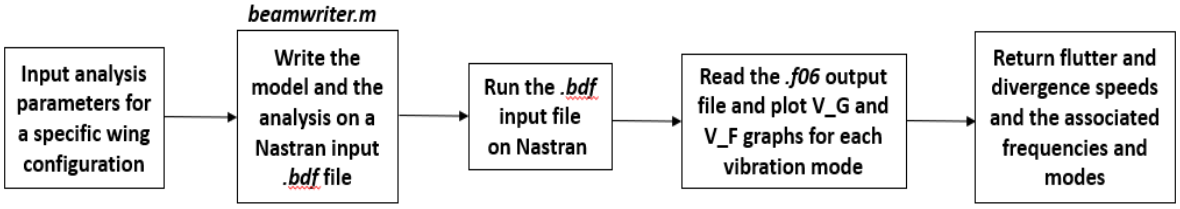

*the beamwriter.m function only writes part of the .bdf input file

Figure 4 - flutter_SOL145.m function flowchart

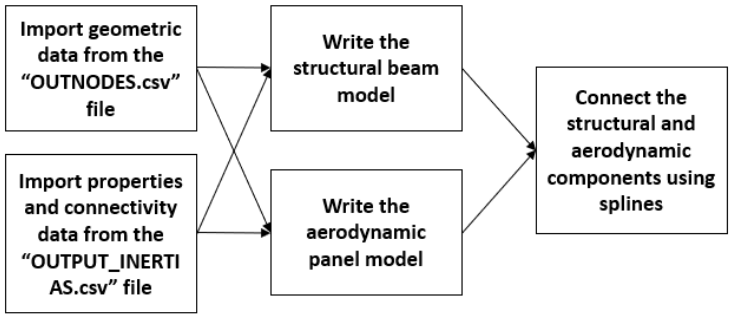

Figure 5 - beamwriter.m function flowchart

4. Results

4.1. Application Case

The application case of this work is a rectangular NACA 0012 wing model with 20 meters of span *b* and variable chord *c* and, as it can be seen in Figure 6, it has an internal structure with a wing-box comprised between 25% and 75% of the chord.

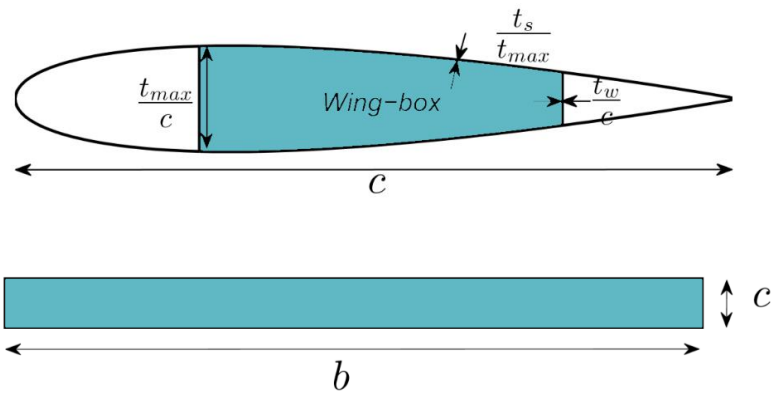

Figure 6 - External and Internal geometries of the wing model

This model is made of aluminum with a Young modulus of 70 GPa, a density of 2700 kg/m^3 and a shear modulus of 27 GPa. In order to evaluate the effect of aspect-ratio, wing span was set fixed to 20 m, while the chord was changed to generate three different values of aspect-ratio *AR*: 12 (*c* = 1.67 m), 20 (*c* = 1 m) and 28 (*c* = 0.71 m). Such geometric modifications change the wing area. For instance, by reducing the chord a smaller wing area *S* and a larger aspect-ratio *AR* were reached. Moreover, since the wing-box parameters such as the thicknesses of the webs and caps are normalized to the chord and airfoil maximum thickness, as the wing chord decreases, the mass and inertia moments also decrease. However, despite the differences in wing area and mass, they still have the same inertia ratio I_2/I_1 (ratio between the two bending stiffnesses, chord EI_2 and flap EI_1) and undergo different deformed states for the same flight conditions. This is what allows a comparison between different flutter prediction methods while considering wing models that present different aeroelastic behavior. A summary of the main characteristics of the considered wings is presented in Table 1.

Table 1 - Main characteristics of three different wing configurations

AR	*c* [m]	*b* [m]	*S* [m^2]	EI_1 [N m^2]	EI_2 [N m^2]	*GJ* [N m^2]	I_2/I_1 [-]	*Mass* [kg]
12	1.67	20.00	33.33	3.76E+06	1.02E+08	3.57E+06	27.1	679.34
20	1.00	20.00	20.00	4.88E+05	1.32E+07	4.63E+05	27.1	244.56
28	0.71	20.00	14.29	1.27E+05	3.44E+06	1.20E+05	27.1	124.78

4.2. The Frequency Domain Method Results

4.2.1 Frequency Domain Tool under different conditions

First, we will show a contrast between three different conditions through which is possible to use the frequency domain tool:

- Condition 1 – Estimating the flutter speed of an undeformed wing at a low airspeed.
- Condition 2 – Estimating the flutter speed of a deformed wing at a low airspeed.
- Condition 3 – Estimating the flutter speed after a convergence cycle, at an airspeed that matches the predicted flutter speed, while considering the wing deformation due to the airspeed.

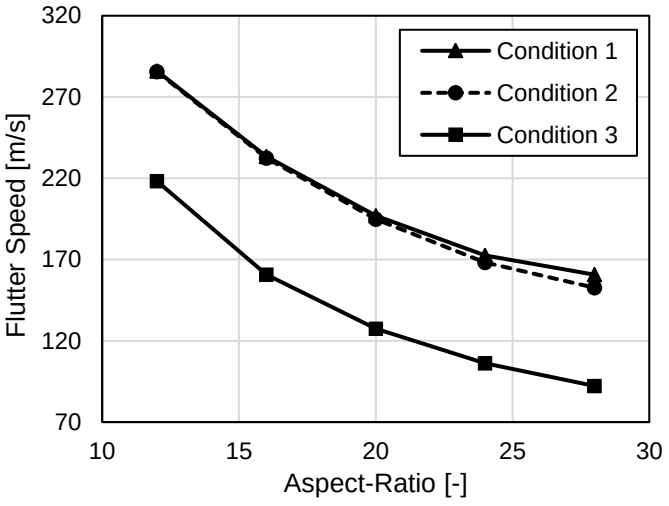

Figure 7 - Flutter speed vs AR

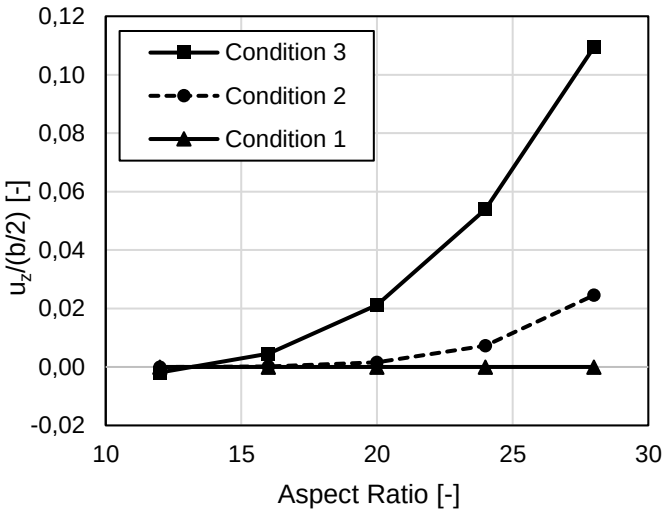

Figure 8 - Dimensionless wing tip displacement vs AR

As expected for all conditions, the predicted flutter speed decreases with an increase in the wing aspect-ratio. While comparing conditions 1 and 2, in Figure 7 it is possible to see that even a slightly deformed wing (at an airspeed of 40 m/s) has an influence in the predicted flutter speed. As expected, the prediction is that a deformed wing would reach the flutter point at a lower speed than an undeformed one. The higher the aspect-ratio, the higher the deformation (as shown in Figure 8) and consequently the larger the difference between predicted flutter speeds.

Regarding condition 3, in Figure 7, we can see that it presents a similar trend to that of condition 2, although slightly steeper because of the higher deformation at a higher airspeed (which is again

shown in Figure 8). Also, for the different aspect-ratios, the flutter and airspeed converge at values that are lower than the one predicted in condition 2.

4.2.2 Frequency Domain Results

The following are the “end product” results obtained through the frequency domain tool (which were addressed above as “condition 3”).

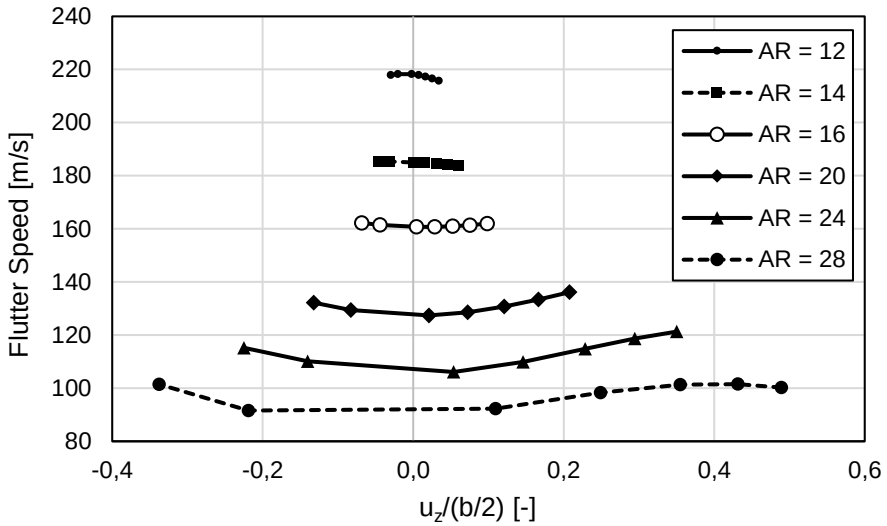

Figure 9 - Predicted flutter speeds and corresponding dimensionless wing tip displacements at the aeroelastic static equilibrium states for wings of different aspect-ratio at different flight conditions (where the angle of attack was swept from -4 degrees to 10

As one can observe from Figure 9, the changes made on the wing to produce different aspect-ratios highlighted the nonlinear of behavior of these flexible wings as the flight conditions change. For low aspect-ratios, such as *AR* = 12, flutter speeds decrease as the dimensionless vertical tip displacement increases caused by the different angles of attack. Then, for an aspect-ratio of 14, the flutter speed is nearly constant with the increase of the vertical tip displacement. Finally, for aspect-ratios higher than 14, the flutter speed increases as the vertical tip displacement increases, inverting the previously observed trend, up to a given point as noted for dimensionless vertical tip displacements above 40% for the a wing aspect-ratio of 28. Another relevant factor to notice is that flutter is predicted to occur at increasing dimensionless tip displacements as the aspect-ratio increases. An explanation to this could be assigned to the fact that the higher flexibility effect exceeds the reduction of the loads due to the lower airspeed.

4.2.3 Flutter Mechanism

Here, we will observe the flutter mechanism of a wing through the analysis of V-G (Velocity-Damping) and V-F (Velocity-Frequency) plots.

Table 2 - Natural frequencies and identified vibration mechanisms of the first few vibration modes of three wings with different aspect-ratios

Mode	*AR* = 12		*AR* = 20		*AR* = 28	
	Frequency [Hz]	*Vibration Mode*	*Frequency [Hz]*	*Vibration Mode*	*Frequency [Hz]*	*Vibration Mode*
1	2.39	1st Flap	1.11	1st Flap	0.67	1st Flap
2	9.46	1st Chord	5.78	1st Chord	3.46	1st Chord
3	14.91	2nd Flap	6.95	2nd Flap	4.16	2nd Flap
4	35.17	1st Torsion	19.44	3rd Flap	11.63	3rd Flap
5	41.65	3rd Flap	23.37	1st Torsion	19.76	1st Torsion

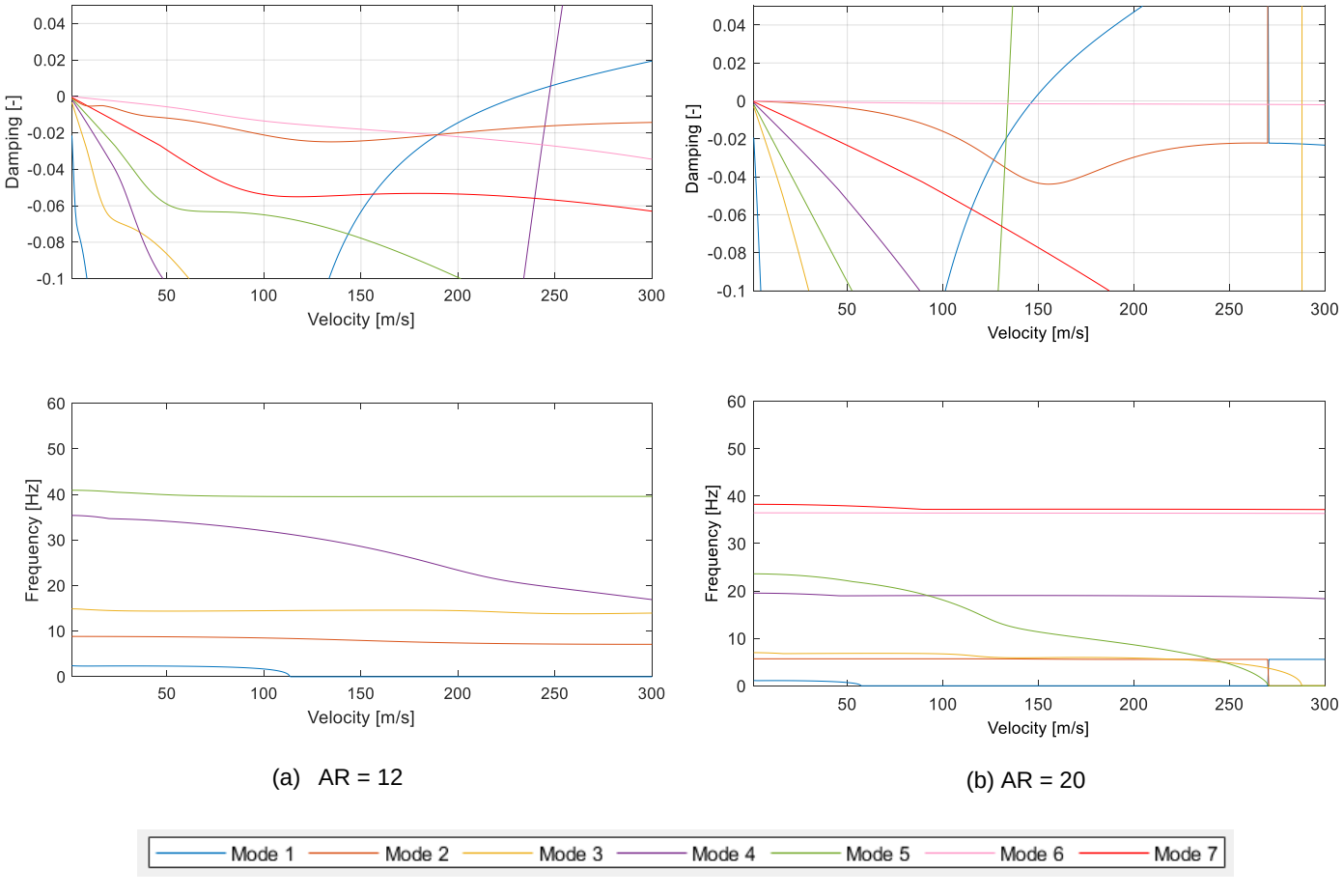

(a) AR = 12

(b) AR = 20

Figure 10 - V-G and V-F plots at the flutter speed boundaries for the wings of aspect-ratios of 12 and 20, at an angle of attack of 6 degrees

By analyzing Figure 10, for the wing of AR = 12, flutter seems to occur when the fourth mode (first torsion) damping becomes positive and its frequency starts to converge with the one of the third mode (second flap), which suggests some mode coupling between these two modes. For the wing of AR = 20, flutter appears to occur when the fifth mode (first torsion) damping becomes positive and its frequency converges with the one of the fourth mode (third flap), suggesting some mode coupling between these two modes. These graphs highlight the nonlinear behavior of the mechanism leading to flutter.

Looking at Table 2, it can be noticed that in wings with aspect-ratios lower than 20, the first torsion mode is the fourth vibration mode and third flap mode is the fifth one, while on wings of aspect-ratio of 20 or above, this tendency switches, and the third flap mode appears before the first

torsion mode. The reason why we think this happens is the fact that as the aspect-ratio increases, the inertia moments change along the wing, leading the wing to become weaker when resisting to flap bending. As expected, all the vibration frequencies decrease, but the flap bending modes are particularly weakened. It is also relevant to note that in all the considered wing models the critical flutter vibration mode seems to be the first torsion mode.

4.3 The Time Domain Method Results

The following table (Table 3) presents a summary of the speed and dimensionless vertical tip displacement values at which flutter was predicted to occur, using the time domain method, for three wings of different aspect-ratios.

Table 3 - : Predicted flutter speed and dimensionless wing tip displacement using the time domain approach

AR	$u_z/(b/2)$ [-]	Flutter Speed [m/s]
12	0.1201	121.27
20	0.6274	113.17
28	0.6778	82.80

4.4 Comparison Between Frequency and Time Domain Methods

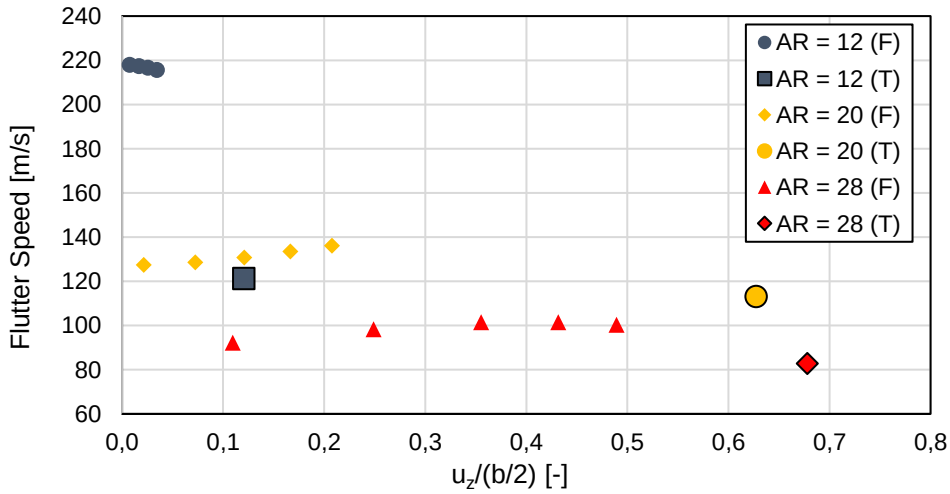

Figure 11 - Flutter speeds and corresponding dimensionless vertical wing tip displacement obtained through frequency and time domain methods

As it was discussed in the previous sections, some trends were found to behave alike in both the frequency and the time domain methods of calculation: the predicted flutter speed decreases as the wing flexibility increases (as a consequence of the aspect-ratio increase); flutter occurs at increasing dimensionless tip displacements as the aspect-ratio increases; the critical flutter mode seems to be the first torsion for all the considered wing models; and it could be said that the predicted flutter mechanisms are nearly the same in both methods (coupling between a torsion and a flap bending modes). However, despite the flutter speed estimated using the frequency domain becoming closer to the one predicted by time domain method as the wing deformation increases, it was not possible to obtain exactly the same flutter speed in both approaches.

Moreover, by analyzing Figure 11, it looks like these predictions using the frequency domain approach might not even be conservative.

Concluding this comparison, it is not possible to infer from these results that the updated frequency domain approach, where the static equilibrium state was used, yields accurate results. Further research is thus needed.

5. Concluding Remarks

In this work, a frequency domain method, where the wing aeroelastically static equilibrium state is used as an input instead of the undeformed wing, was presented and compared with a time domain approach for the flutter speed prediction of high aspect-ratio wings. It could be observed that some trends seemed to converge and were identified as behaving alike in both cases. However, despite the solutions obtained with the two methods becoming closer as the wing deformation increases, it was not possible to predict exactly the same flutter speed result in both techniques. Still, it can be concluded that the developed frequency domain tool managed to produce consistent results at a low computational cost, and it can prove useful in situations where its low computational cost would be relevant. For example, in optimization problems, the frequency domain tool could be used to evaluate relative predicted flutter speeds in a comparison between different wing models. A suggestion for the future could be to refine the structural component of the frequency domain tool. For example, a change that could be interesting and easy to implement would be to replace the Euler-Bernoulli beam model with the Timoshenko one. A more complex upgrade would be to change the beam model for a plate model. The most laborious improvement to the process would probably be to generate experimental data in order to validate the flutter speed and flutter mechanism predictions.

References

[1] J. E. Cooper and M. Y. Harmin, “Aeroelastic behaviour of a wing including geometric nonlinearities,” Aeronautical Journal, vol. 115, no. 1174, pp. 767-777, 2011.

[2] F. Petrini, F. Giuliano e F. Bontempi, “Comparison of time domain techniques for the evaluation of the response and the stability in long span suspension bridges,” Computers & Structures, nº 85, p. 1032–1048, 2007.

[3] L. Salvatori and C. Borri, “Frequency- and time-domain methods for the numerical modeling of full-bridge aeroelasticity,” Computers & Structures, no. 87, pp. 675-687, 2007.

[4] L. Salvatori and P. Spinelli, “Effects of structural nonlinearity and along-span wind coherence on suspension bridge aerodynamics: some numerical simulation results,” Journal of Wind Engineering and Industrial Aerodynamics, vol. 94, no. 5, p. 415–430, 2006.

[5] S. J. Hulshoff, Aeroelasticity (version 11.1): AE4930, Delft: TU Delft, Faculty of Aerospace Engineering, 2011.

[6] A. Suleman, F. Afonso, J. Vale, E. Oliveira and F. Lau, “Non-linear aeroelastic analysis in the time domain of high-aspect-ratio wings: Effect of chord and taper-ratio variation,” The Aeronautical Journal, vol. 121, no. 1235, pp. 21-53, 2017.

[7] F. Afonso, G. Leal, J. Vale, E. Oliveira, F. Lau and A. Suleman, “The effect of stiffness and geometric parameters on the nonlinear aeroelastic performance of high aspect ratio wings,” Proc IMech E Part G: J Aerospace Engineering, vol. 231, no. 10, pp. 1824-1850, 2017.

[8] J. N. Reddy, An introduction to the finite element method, 3rd. ed. ed., New York: McGraw-Hill Education, 2005.

[9] E. Albano and W. P. Roden, A Doublet-Lattice method for calculating lift distributions on oscillating surfaces in subsonic flows, Hawthorne, USA: Northrop Corporation, Norair Division,, 1969.